On the Relation Between Beam Coupling and Feed Coupling in Wideband Antenna Arrays

Ozzola, Riccardo; Cavallo, Daniele; Neto, Andrea

DOI
10.1109/TAP.2021.3090536

Publication date
2022

Document Version
Accepted author manuscript

Published in
IEEE Transactions on Antennas and Propagation

This article has been accepted for publication in a future issue of this journal, but has not been fully edited. Content may change prior to final publication. Citation information: DOI 10.1109/TAP.2021.3090536, IEEE Transactions on Antennas and Propagation

On the Relation Between Beam Coupling and Feed Coupling in Wideband Antenna Arrays

Riccardo Ozzola, *Student Member, IEEE,* Daniele Cavallo, *Senior Member, IEEE*, Andrea Neto, *Fellow, IEEE*

***Abstract*—We present a study on the beam coupling in radiating structures that support multiple simultaneous beams. The formation of multiple beams is relevant in modern wireless communication applications, when diverse data streams can be sent from a single transmitter to users located in different directions. General expressions are provided that relate the coupling between radiated beams to the associated current distributions on the radiating aperture. When expanding the currents in terms of basis functions, the beam coupling can be also written in terms of coupling contributions due to each pair of basis functions. The analysis is applied to antenna arrays with different levels of mutual coupling between the array elements. More specifically, arrays of resonant elements, characterized by very low mutual coupling, are compared with arrays of connected elements, which are strongly coupled. We show that, even for very high level of mutual coupling between individual array elements, it is possible to obtain orthogonal beams if the total current distributions associated with the beams are uncoupled.**

***Index Terms*—Antenna arrays, beam coupling factor, multiple beams, mutual coupling, wideband arrays.**

I. Introduction

WIRELESS communications in the near future will heavily rely on the possibility to transmit and receive multiple data streams through directive beams connecting the base station with different users (Fig. 1). With the advent of 5G communications and the planning for future 6G networks, antennas will focus the radiation in smaller angular regions with the aim to improve the energy and spectral efficiency, while reducing interference levels. In such a communication scenario, base stations will be equipped with phased array antennas serving several distributed users simultaneously by means of multiple adaptively steered beams. Thus, multibeam antennas are regarded as a key technology for enabling massive multiple-input and multiple-output (MIMO) and high speed mobile networks [1]–[3].

In the 1960s, the first theoretical works on the multibeam generation from a single radiating aperture were introduced [4]–[6]. More specifically, beam coupling factors to quantify the orthogonality between beams were defined by Stein in [6]. Stein's theory linked the coupling between two beams generated by a radiating aperture to the coupling between feed lines (or beamformer structures) associated with those beams. Later on, these same coupling coefficients were named envelope correlation between antenna patterns and used in MIMO communication scenarios [7]–[10], as a statistical value indicating the similarity in the voltages received by different antennas in the presence of multipath. In absence of losses, when associating each beam with a feeding structure, the coupling between two antenna beams can be approximated in terms of the impedance or scattering matrix between the feeds [8].

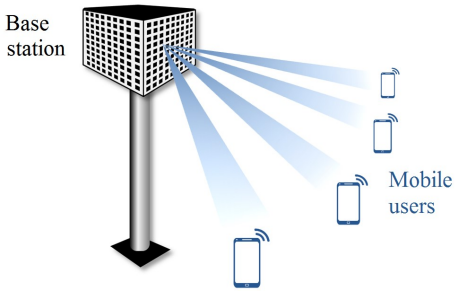

Fig. 1. Wireless base station simultaneously connecting with several mobile users.

In MIMO architectures, mutual coupling between antennas is typically regarded as a limitation, as it is associated with reduced system capacity [11]–[14]. For this reason, several techniques have been employed for the reduction of mutual coupling [15], [16] or the compensation of its effects [17]–[19]. However, these works typically refer to configurations in which the beam orthogonality is intended at the level of the radiation patterns from individual elements of the array. On the contrary, when each beam is collectively generated by all antennas, the beam coupling is not directly related to the coupling between individual elements, but to the coupling between beamforming structures [6]. In these cases, the role of mutual coupling between individual elements in the performance of the multibeam systems remains unclear. For example, in [20] it was shown that a nonzero mutual coupling level maximizes the gain in arrays when the elements are simultaneously excited. More recently, MIMO concepts based on high mutual coupling arrays have been proposed in [21].

The main scope of this paper is to clarify how the inter-element mutual coupling affects the capability of creating multiple simultaneous beams with a single phased array. To this aim, we evaluate the beam coupling coefficients for arrays of dipoles, comparing two canonical geometries: linear arrays of collinear resonant dipoles, for which the mutual coupling is relatively low, and linear arrays of connected dipoles, characterized by high mutual coupling. Moreover, examples of

Manuscript received Month DD, YYYY; revised Month DD YYYY. First published Month DD, YYYY; current version published Month DD, YYYY.

R. Ozzola, D. Cavallo and A. Neto are with the Microelectronics Department of the Electrical Engineering, Mathematics and Computer Science Faculty, Delft University of Technology, 2628 CD Delft, The Netherlands (e-mail: R.Ozzola-1@tudelft.nl).

Color versions of one or more of the figures in this paper are available online at http://ieeexplore.ieee.org.

Digital Object Identifier XX.XXXX/TAP.XXXX.XXXXXXXX

This article has been accepted for publication in a future issue of this journal, but has not been fully edited. Content may change prior to final publication. Citation information: DOI 10.1109/TAP.2021.3090536, IEEE Transactions on Antennas and Propagation

two dimensional arrays are presented, namely a narrowband array of patches and a more wideband array of connected slots with dielectric superstrate.

For the investigation, we first express the coupling between two beams in terms of the electric current distributions associated with each beam. The resulting expression contains a coupling integral between the two currents similar to a mutual impedance, but with a kernel that is a singularity-free Green's function [10]. By expanding the currents in terms of basis functions, the beam coupling can be also written as a weighted sum of coupling contributions between each pair of basis functions. The derived expressions can be applied to the different arrays, to quantify the effect of different levels of mutual coupling on the beam orthogonality. We give a few examples of multibeam arrays for which the coupling between beams can be weakly dependent on the level of mutual coupling between individual elements of the array.

Since high mutual coupling between ports is a characterizing feature of all wideband wide scanning arrays, this finding opens the possibilities to largely increase the bandwidth and scan performance of MIMO arrays. In fact, wide bandwidth is an important aspect of future wireless communication. When more and more frequency bands will be used for different services, having a single narrowband antenna for each subband will become unfeasible for cost and space occupation. For this reason, the use of wideband arrays that can cover simultaneously multiple bands will become increasingly important.

II. Beam-Coupling Factor

Let us consider a radiating aperture, as depicted in Fig. 2, which radiates N_b beams, with indexes $n \in \{1, \cdots, N_b\}$. Each beam is characterized by an electric field $\mathbf{e}_n(\mathbf{r})$, radiated by an associated electric current distribution $\mathbf{j}_n$, where $\mathbf{r} \equiv (r, \theta, \phi)$ is a generic point in the far-field with radial distance r, elevation angle θ and azimuthal angle ϕ. The electric field for the n-th beam is given by

$$\mathbf{e}_n(\mathbf{r}) = \mathbf{E}_n(\hat{\mathbf{k}}) \frac{e^{-jkr}}{r} \tag{1}$$

where k is the free space propagation constant and $\mathbf{E}_n(\hat{\mathbf{k}})$ represents the far field radiation pattern, which is a function of the angular direction $\hat{\mathbf{k}} = \sin\theta\cos\phi\hat{\mathbf{x}} + \sin\theta\sin\phi\hat{\mathbf{y}} + \cos\theta\hat{\mathbf{z}}$. The radiation pattern can be related to the electric current distributions by

$$\mathbf{E}_n(\hat{\mathbf{k}}) = -\frac{jk\zeta}{4\pi}[\underline{\underline{\mathbf{I}}} - \hat{\mathbf{k}}\hat{\mathbf{k}}] \cdot \mathbf{J}_n(\hat{\mathbf{k}}) \,. \tag{2}$$

In (2), $\zeta = 120\pi$ is the free space characteristic impedance, $\underline{\underline{\mathbf{I}}}$ is the identity dyad. The function $\mathbf{J}_n$ is the spatial Fourier transform of $\mathbf{j}_n$, given by

$$\mathbf{J}_n(\hat{\mathbf{k}}) = \iint_{S_n} \mathbf{j}_n(\mathbf{r}') e^{jk\hat{\mathbf{k}}\cdot\mathbf{r}'} d\mathbf{r}' \tag{3}$$

where S_n refers to the domain in which the n-th current distribution $\mathbf{j}_n$ differs from 0.

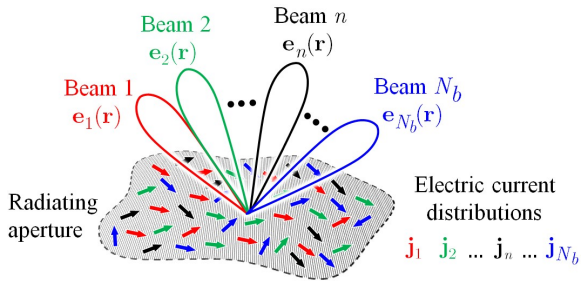

Fig. 2. Radiating aperture generating N_b beams, characterized by the electric fields $\mathbf{e}_n$, associated with the electric current distributions $\mathbf{j}_n$.

A. General Definition of Beam Coupling

As formalized in [6], the cross coupling between any pair of beams with patterns $\mathbf{E}_n$ and $\mathbf{E}_{n'}$ can be expressed as

$$c_{nn'} = \frac{\iint_{4\pi} \mathbf{E}_n^*(\hat{\mathbf{k}}) \cdot \mathbf{E}_{n'}(\hat{\mathbf{k}}) d\hat{\mathbf{k}}}{\sqrt{\iint_{4\pi} \left|\mathbf{E}_n(\hat{\mathbf{k}})\right|^2 d\hat{\mathbf{k}}} \sqrt{\iint_{4\pi} \left|\mathbf{E}_{n'}(\hat{\mathbf{k}})\right|^2 d\hat{\mathbf{k}}}} \,. \tag{4}$$

The double integral at the numerator of (4) represents an inner product between two radiation patterns in the angular domain. The terms at the denominator are normalization factors so that the modulus of the coupling factor satisfies the following condition: $0 \leq |c_{nn'}| \leq 1$. The notation used for the integrals, for a generic function f, is explicitly related to the angular variables by

$$\iint_{4\pi} f(\hat{\mathbf{k}}) d\hat{\mathbf{k}} = \int_0^{2\pi} \int_0^{\pi} f(\theta, \phi) \sin\theta d\theta d\phi \,. \tag{5}$$

By substituting (2) in (4) and following the algebraic steps reported in Appendix A, the beam coupling factor can also be expressed in terms of the currents spectral distributions [9]:

$$c_{nn'} = \frac{R_{nn'}}{\sqrt{R_{nn}}\sqrt{R_{n'n'}}} \tag{6}$$

where

$$R_{nn'} = \frac{k^2\zeta}{16\pi^2} \iint_{4\pi} \mathbf{J}_n^*(\hat{\mathbf{k}}) \cdot [\underline{\underline{\mathbf{I}}} - \hat{\mathbf{k}}\hat{\mathbf{k}}] \cdot \mathbf{J}_{n'}(\hat{\mathbf{k}}) d\hat{\mathbf{k}} \,. \tag{7}$$

To give an interpretation of the term $R_{nn'}$, it is convenient to express it in the spatial domain by using (3), leading to

$$R_{nn'} = -\iint_{S_n} \iint_{S_{n'}} \mathbf{j}_n^*(\mathbf{r}) \cdot \mathbf{g}^{\text{vis}}(\mathbf{r} - \mathbf{r}') \cdot \mathbf{j}_{n'}(\mathbf{r}') d\mathbf{r}' d\mathbf{r} \tag{8}$$

where we defined a 'visible' Green's function as

$$\mathbf{g}^{\text{vis}}(\mathbf{r} - \mathbf{r}') = \frac{-k^2\zeta}{16\pi^2} \iint_{4\pi} [\underline{\underline{\mathbf{I}}} - \hat{\mathbf{k}}\hat{\mathbf{k}}] e^{-jk\hat{\mathbf{k}}\cdot(\mathbf{r}-\mathbf{r}')} d\hat{\mathbf{k}}. \tag{9}$$

It is worth noting that the expression (8) resembles a mutual impedance between the two current distributions, where the inner product defines a norm as in [22]:

$$Z_{nn'} = -\iint_{S_n} \iint_{S_{n'}} \mathbf{j}_n^*(\mathbf{r}) \cdot \mathbf{g}(\mathbf{r} - \mathbf{r}') \cdot \mathbf{j}_{n'}(\mathbf{r}') d\mathbf{r}' d\mathbf{r} \,. \tag{10}$$

This article has been accepted for publication in a future issue of this journal, but has not been fully edited. Content may change prior to final publication. Citation information: DOI 10.1109/TAP.2021.3090536, IEEE Transactions on Antennas and Propagation

The function $\mathbf{g}$ is the free-space dyadic Green's function which relates the electric field to the electric current. Comparing (10) with (8), one can note that, while $\mathbf{g}$ is obtained by integrating the spectral Green's function over the entire spectrum, the visible Green's function $\mathbf{g}^{\text{vis}}$ results from an integration only on the visible spectrum as in (9). Moreover, the visible Green's function does not exhibit singularities even for co-located sources, since does not include the term $|\mathbf{r}-\mathbf{r}'|^{-1}$ of the standard free-space Green's function. This can be observed by realizing that, as demonstrated in appendix B, the integral on the visible spectrum in (9) can be expressed as

$$\underline{\underline{\mathbf{g}}}^{\text{vis}}(\mathbf{r}) = -\frac{\zeta}{4\pi}[k^2\underline{\underline{\mathbf{I}}} + \nabla\nabla]\text{sinc}(kr). \tag{11}$$

The quantity in (8) represents a 'visible' mutual impedance that depends only on how the two currents interact with their far-field radiation patterns. It can be demonstrated that, for real-valued current distributions, normalized so that they are equal to 1 at the port terminals, $R_{nn'}$ coincide with the mutual resistance, i.e. $R_{nn'} = Re\{Z_{nn'}\}$ [24].

B. Expansion of Electric Currents with Basis Functions

Often in antenna problems the current distributions are not available beforehand, but they have to be evaluated by means of numerical methods. For instance, one can expand the n-the current distribution in a sum of basis functions, as typically done in Method of Moments solutions:

$$\mathbf{j}_n(\mathbf{r}) = \sum_m i_{m,n}\mathbf{b}_m(\mathbf{r}) \tag{12}$$

where $\mathbf{b}_m(\mathbf{r})$ is the m-th sub-domain basis function and $i_{m,n}$ is its corresponding weight. If all basis functions are equal, (12) becomes

$$\mathbf{j}_n(\mathbf{r}) = \sum i_{m,n}\mathbf{b}(\mathbf{r}-\mathbf{r}_m) \tag{13}$$

where $\mathbf{r}_m$ is the center of the m-th basis function. The Fourier transform of $\mathbf{j}_n(\mathbf{r})$ can be written as follows:

$$\mathbf{J}_n(\hat{\mathbf{k}}) = \sum_m i_{m,n}\mathbf{B}(\hat{\mathbf{k}})e^{jk\hat{\mathbf{k}}\cdot\mathbf{r}_m} \tag{14}$$

where $\mathbf{B}(\hat{\mathbf{k}})$ is the Fourier transform of $\mathbf{b}(\mathbf{r})$. By substituting (14) in (8), one obtains

$$R_{nn'} = \sum_m i^*_{m,n}\sum_{m'} i_{m'n'}R_{mm'}. \tag{15}$$

where

$$R_{mm'} = \frac{k^2\zeta}{16\pi^2}\iint_{4\pi}\mathbf{B}^*(\hat{\mathbf{k}})\cdot[\underline{\underline{\mathbf{I}}}-\hat{\mathbf{k}}\hat{\mathbf{k}}]\cdot\mathbf{B}(\hat{\mathbf{k}})e^{-jk\hat{\mathbf{k}}\cdot(\mathbf{r}_m-\mathbf{r}_{m'})}d\hat{\mathbf{k}}\,. \tag{16}$$

The beam coupling in (6) can be then expressed as

$$c_{nn'} = \frac{\underline{\mathbf{i}}_n^H\,\underline{\underline{\mathbf{R}}}\,\underline{\mathbf{i}}_{n'}}{\sqrt{\underline{\mathbf{i}}_n^H\,\underline{\underline{\mathbf{R}}}\,\underline{\mathbf{i}}_n}\sqrt{\underline{\mathbf{i}}_{n'}^H\,\underline{\underline{\mathbf{R}}}\,\underline{\mathbf{i}}_{n'}}} \tag{17}$$

where $\underline{\mathbf{i}}_n$ are the weights of n-th current expansion, $\underline{\underline{\mathbf{R}}}$ is the matrix whose entries are defined in (16) and H indicates the Hermitian transpose. As already pointed out earlier, for real-valued basis functions, the matrix $\underline{\underline{\mathbf{R}}}$ is equal to real part of the method of moments impedance matrix. However, $c_{nn'}$ has still complex value, since it depends on the complex amplitudes of the basis functions associated with the two beams, $\underline{\mathbf{i}}_n$ and $\underline{\mathbf{i}}_{n'}$.

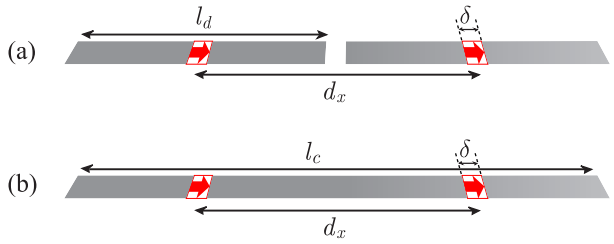

Fig. 3. Geometry for: (a) two center-fed collinear dipoles, with length l_d, distance between centers d_x, delta-gap size δ; (b) two connected dipoles, with total length l_c and distance between feeds d_x.

III. Application to Dipole Arrays

To quantify how the mutual coupling in antenna arrays affects the beam orthogonality, we evaluate the expressions given in the previous section for arrays of dipoles. For the sake of simplicity, we first analyze and compare two simple geometries: an array of two collinear dipoles, as shown in Fig. 3(a), and an array of two connected dipoles, depicted in Fig. 3(b). This choice is motivated from the fact that two aligned dipoles are typically poorly coupled because of radiation null along their axis. On the contrary, connected dipoles are characterized by high mutual coupling, since the current can flow from one element to the other through the electrical connection.

A method of moments analysis, similar to the one described in [26] has been implemented to apply the expression of the beam coupling from (17). The geometrical parameters are chosen as $d_x = 0.45\,\lambda_0$, $w = \delta = 0.1\,\lambda_0$, $l_d = 0.4\,\lambda_0$ and $l_c = 0.85\,\lambda_0$, where λ_0 is the wavelength at 10 GHz.

A. Comparison between Two-Element Arrays of Disconnected and Connected Dipoles

The reflection coefficient and the mutual coupling between the two elements of the array is shown in Fig. 4, for both disconnected and connected dipoles. The S-parameters are normalized to load impedances equal to $70\,\Omega$ for the disconnected dipole and $150\,\Omega$ for the connected dipole. It can be observed that, for the separated dipoles in Fig. 4(a), the $|S_{12}|$ peaks at around 10 GHz with a value of -12 dB. Moreover, the disconnected dipoles exhibit a narrow bandwidth due to the typical resonant nature of the radiating element. On the contrary, higher levels of mutual coupling occur for connected dipoles in Fig. 4(b), higher than -8 dB over the large bandwidth of investigation. It is well known that, by electrically connecting the dipoles, the S-parameters become more frequency independent, achieving wideband impedance matching [27].

The beam coupling coefficient c_{12} is also evaluated as a function of frequency in Fig. 5. In this section, we assume that the two beams are obtained with one of the two elements active

This article has been accepted for publication in a future issue of this journal, but has not been fully edited. Content may change prior to final publication. Citation information: DOI 10.1109/TAP.2021.3090536, IEEE Transactions on Antennas and Propagation

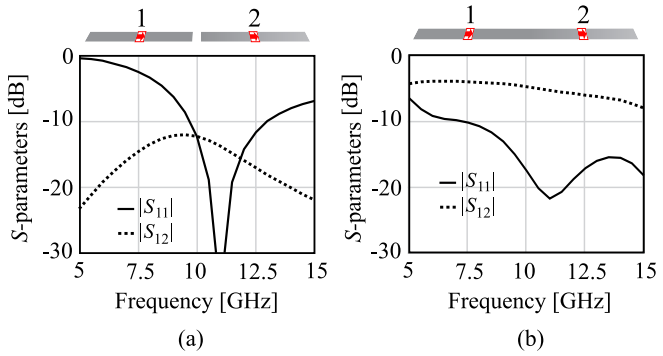

Fig. 4. S_{11} and S_{12} for 2-element arrays of (a) resonant dipoles and (b) connected dipoles.

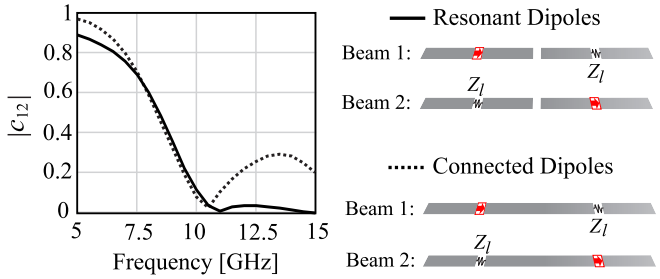

Fig. 5. c_{12} for 2-element array of resonant and connected dipoles. The beam coupling is intended between beams obtained with one of the two elements in the array active and the other passively terminated and vice versa.

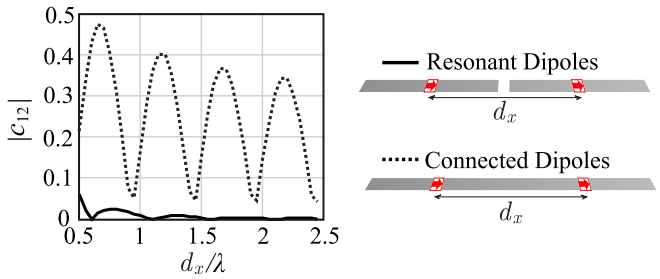

Fig. 6. c_{12}, calculated at 10 GHz, versus the inter-element distance for 2-element array of resonant and connected dipoles; λ is the wavelength at 10 GHz.

and the other terminated on a resistive load. The frequency dependence of the beam coupling is similar for the two structures, but the connected array exhibits higher values of c_{12}, due to the higher mutual coupling.

From Fig. 5, the values of c_{12} are shown to be close to 0 for both structures at around 11 GHz, which corresponds to a distance between feeds of around half wavelength. To better highlight this aspect, we report in Fig. 6 the beam coupling for a fixed frequency (10 GHz), but varying the distance of the two elements, for both resonant and connected dipoles. The curves oscillate as a function of the frequency creating a interference pattern that depends on the electrical distance between elements. Much higher levels are obtained for the connected dipole elements, because of the high mutual coupling.

Therefore, in the configuration in which the two elements are to be used independently, i.e. when one beam is associated

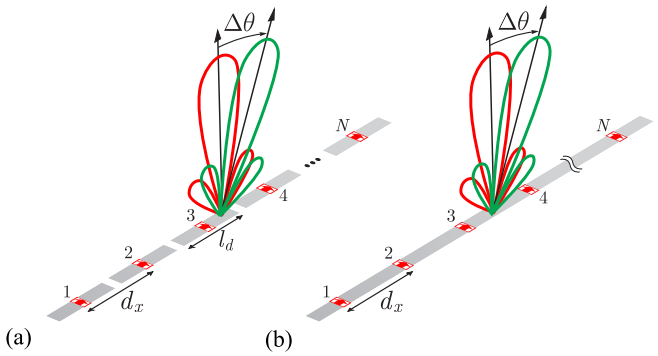

Fig. 7. N-element linear array of resonant and connected dipoles. The array generates two beams, pointing at broadside and $\Delta\theta$, respectively.

with one feeding gap, high inter-element mutual coupling yields high beam coupling. Indeed, in this case c_{12} is closely related to the mutual impedance, and thus directly proportional to the levels of mutual coupling. In this configuration, although connected arrays are intended to be used over a wide frequency range, low levels of c_{12} can be achieved only over a narrow frequency band.

B. Linear Arrays Generating Multiple Directive Beams

Another case possibly even more important to investigate is when the array comprises more the 2 elements (arbitrary number of elements N) and the beams are collectively generated by all elements. For this study, we assume that such an array generates two beams, one fixed pointing at broadside (beam 1) and the other pointing at a varying angular direction $\Delta\theta$ (beam 2). Thus, the array is fed simultaneously with two voltage distributions $\mathbf{v}_1$ and $\mathbf{v}_2$, given by

$$v_{1,n} = 1 \qquad \text{for } n \in [1, N] \qquad (18)$$

$$v_{2,n} = e^{-jknd_x \sin(\Delta\theta)} \qquad \text{for } n \in [1, N] \qquad (19)$$

assuming that the elements are located on the x-axis in the reference system. The coupling between these two beams is shown in Fig. 8, for both resonant and connected dipoles, as a function of the separation between the beams $\Delta\theta$ and for different number of elements. The geometrical parameters are $d_x = 0.45\,\lambda_0$, $l_d = 0.4\,\lambda_0$, where λ_0 is the wavelength at the calculation frequency.

The coupling is equal to 1 for total overlap between beams ($\Delta\theta = 0°$) and decreases for larger separation of the pointing angles. The oscillations are due to the interference between sidelobes of the two patterns. Zeros of the coupling occur when the maximum of the main lobe of one beam is aligned with the null of the other. This corresponds to $\Delta\theta$ equal to one half of the first null beamwidth. For smaller arrays, the beams overlap for a larger range of $\Delta\theta$, due to the wider beamwidth.

It can be noted from Fig. 8 that the coupling curves for the resonant and connected dipoles are very similar, despite the different mutual-coupling levels.

To reduce the beam coupling after the first null, the side lobes of the pattern can be reduced with a tapered illumination of the array. The coupling in Fig. 15(a) refers to arrays of 16 elements with a Gaussian amplitude distribution with edge

This article has been accepted for publication in a future issue of this journal, but has not been fully edited. Content may change prior to final publication. Citation information: DOI 10.1109/TAP.2021.3090536, IEEE Transactions on Antennas and Propagation

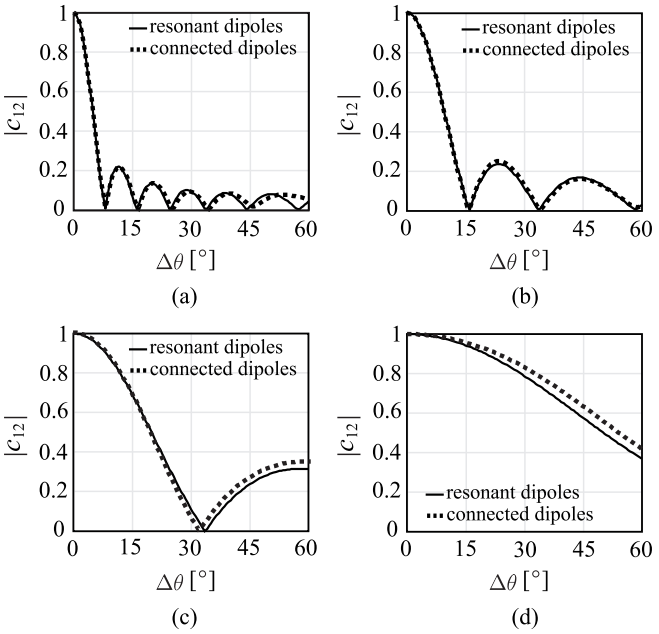

Fig. 8. Beam coupling between two beams, pointing at broadside and $\Delta\theta$, respectively, for linear array of resonant and connected dipoles with (a) $N = 16$, (b) $N = 8$, (c) $N = 4$ and (d) $N = 2$.

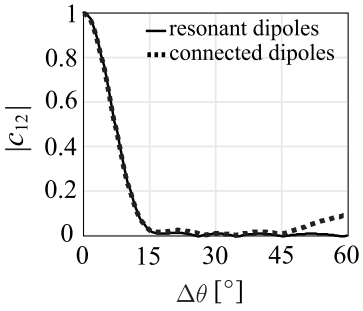

Fig. 9. Beam coupling between two beams, pointing at broadside and $\Delta\theta$, respectively, for linear array of resonant and connected dipoles with $N = 16$ and Gaussian tapered illumination with edge taper of -10 dB.

taper of -10 dB. The coupling remains very low for the low-coupled dipoles for $\Delta\theta > 20°$. On the contrary, the connected array exhibit similar coupling up to $\Delta\theta > 50°$, but increased values for larger scanning of the beam. The scanning above $50°$ yields some mismatch and aberrations in the patterns, as shown in Fig. 15(b), which causes the raise in coupling. In fact the impedance of the array is not anymore well matched for large scanning, and the impedance varies for each element of the array due to finite edge effects in connected dipoles [28].

IV. Examples of Planar Arrays

In this section, we analyze more realistic examples of two-dimensional planar arrays, simulated using a full-wave electromagnetic solver. Two different structures are compared: an array of patches and an array of connected slots, both consisting of 8×8 elements. The two arrays have the same unit cell size, defined by $d_x = d_y = 0.5\,\lambda_0$, where λ_0 is the wavelength at 10 GHz. The unit cells are shown in Fig. 10. The

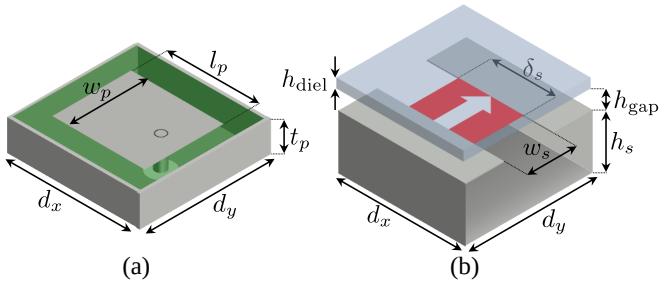

Fig. 10. Unit cell of (a) patch array and (b) connected slot array, with characteristic geometrical parameters.

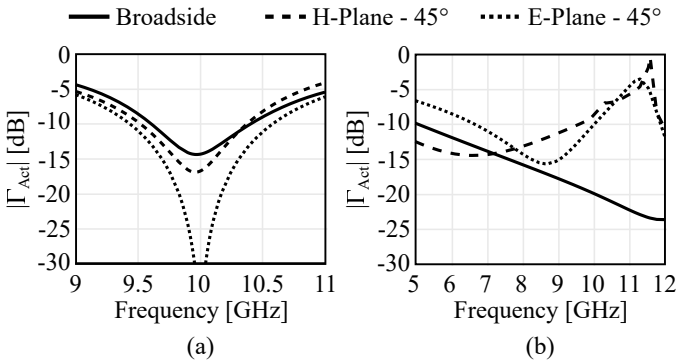

Fig. 11. Active reflection coefficient of the infinite array of (a) patches, and (b) connected slots for broadside and scanning up to $45°$ on the main planes.

patch in Fig. 10(a) is backed by a metal cavity, filled with a dielectric of relative permittivity $\varepsilon_r = 2.33$ and thickness $t_p = 2$ mm. The vertical metal walls of the cavity have been added at the contour of the unit cell to prevent the propagation of surface waves. The other dimensions are $l_p = 8.8$ mm and $w_p = 7.9$ mm. The patch is fed by a vertical pin with diameter of 1.1 mm and the coaxial feed is normalized to a line of $42.5\,\Omega$. The connected slot unit cell is depicted in Fig. 10(b) and is characterized by slot width $w_s = 0.2\,\lambda_0$, fed by a δ-gap generator with size $\delta_s = 0.25\,\lambda_0$, and backed by a ground plane at a distance $h_d = 0.25\,\lambda_0$. Vertical walls have been inserted between the ground plane and the array on the E-plane to improve scanning performance. Moreover the array is loaded with a wide angle impedance matching layer (WAIM), that is a thin dielectric layer of relative permittivity $\varepsilon_r = 5$, $h_{\text{diel}} = 1$ mm, and placed at a distance $h_{\text{gap}} = 2.5$ mm from the array. The port impedance is normalized to $150\,\Omega$.

As shown in Fig. 11,the two unit cells are matched when scanning up to $45°$ on the main planes, but while the array of patches can operate on the band 9.5-10.5 GHz, the connected array is matched over a larger bandwidth, between 7 and 10 GHz. Finite array simulations with 8×8 elements for both structures (see Fig. 12) have been performed with CST. The mutual coupling levels for the two arrays are shown in Fig. 13, between element ports in the center of the array, according to the indexing specified in Fig. 12. It can be observed that a higher level of mutual coupling is obtained for the connecting slots, which is desired to provide a large operational bandwidth.

The beam coupling between a beam pointing to broadside

This article has been accepted for publication in a future issue of this journal, but has not been fully edited. Content may change prior to final publication. Citation information: DOI 10.1109/TAP.2021.3090536, IEEE Transactions on Antennas and Propagation

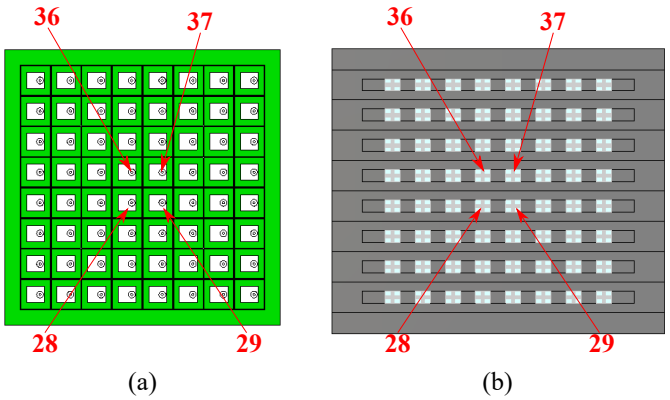

Fig. 12. S parameters of the 8×8 array of (a) patches and (b) connected slots.

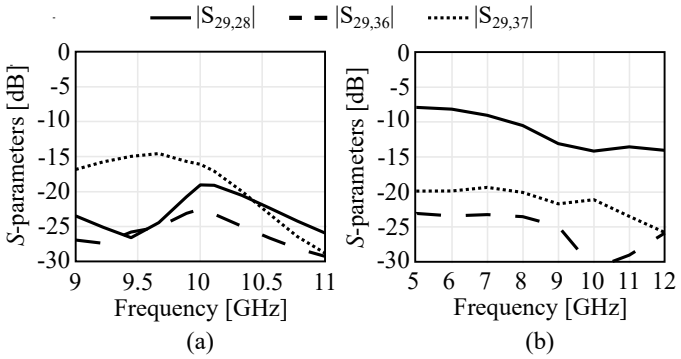

Fig. 13. S parameters of the 8×8 array of (a) patches and (b) connected slots.

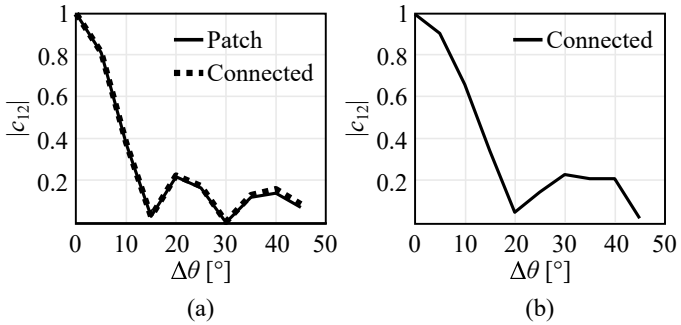

Fig. 14. Beam coupling between two beams, pointing at broadside and $\Delta\theta$, respectively, for 8×8 planar arrays of resonant patches and connected slots at (a) $f = 10\,\text{GHz}$, and $f = 7\,\text{GHz}$.

and a beam pointing to $\Delta\theta$ is presented for the two arrays in Fig. 14 as a function of $\Delta\theta$, at 10 GHz for both arrays and at 7 GHz for the connected slots only. It is evident that, despite the different inter-element coupling levels, the beam coupling values remain comparable in all cases, since they are mainly determined by the beamwidth and the sidelobe level of the radiation patterns.

V. Conclusions

We presented a study on the beam coupling factor in multibeam arrays. The coupling coefficients were expressed in term of current distributions, mutual impedance and inter-element mutual coupling. The study dealt with arrays of dipoles, more specifically comparing resonant dipoles with connected dipoles. The latter are known to have much higher level of mutual coupling, which is typically used to enlarge the bandwidth of operation.

When using the array in the one-beam-per-feed configuration, the coupling between elements is directly related to beam coupling, thus is not desired. However, when different beams are generated by the entire 'active' array, the beams correlation is mainly determined by the beam overlap and is weakly dependent on the mutual coupling. We showed that the beams can remain uncoupled even with high inter-element coupling, as long as the beam do not overlap and the active impedance is well behaved. Example of planar arrays are also given to support this claim.

The finding of this article are relevant for the potential exploitation of wideband arrays in multi-beam communication, which can enable enhanced capability in future wireless networks.

Appendix A
Simplification of the Coupling Integrals

In the present Appendix, we intend to prove that the product between two radiation patterns satisfies the following identity:

$$[\underline{\underline{\mathbf{I}}} - \hat{\mathbf{k}}\hat{\mathbf{k}}] \cdot \mathbf{J}_{n'} \cdot [\underline{\underline{\mathbf{I}}} - \hat{\mathbf{k}}\hat{\mathbf{k}}] \cdot \mathbf{J}_n^* = \mathbf{J}_{n'} \cdot [\underline{\underline{\mathbf{I}}} - \hat{\mathbf{k}}\hat{\mathbf{k}}] \cdot \mathbf{J}_n^* \qquad (20)$$

where we omitted the dependence of the spectral current distributions $\mathbf{J}_n$ and $\mathbf{J}_{n'}$ on $\hat{\mathbf{k}}$ to maintain a compact notation. By expanding the dyadic products on the left hand side, one obtains:

$$\mathbf{J}_{n'} \cdot \mathbf{J}_n^* - \mathbf{J}_{n'} \cdot \hat{\mathbf{k}}\hat{\mathbf{k}} \cdot \mathbf{J}_n^* - \hat{\mathbf{k}}\hat{\mathbf{k}} \cdot \mathbf{J}_{n'} \cdot (\mathbf{J}_n^* - \hat{\mathbf{k}}\hat{\mathbf{k}} \cdot \mathbf{J}_n^*) . \qquad (21)$$

Since the term $(\mathbf{J}_n^* - \hat{\mathbf{k}}\hat{\mathbf{k}} \cdot \mathbf{J}_n^*)$ only selects the transverse components of $\mathbf{J}_n^*$ that are not aligned with $\hat{\mathbf{k}}$, whereas the term $(\hat{\mathbf{k}}\hat{\mathbf{k}} \cdot \mathbf{J}_{n'})$ is parallel to $\hat{\mathbf{k}}$, one can note that

$$\hat{\mathbf{k}}\hat{\mathbf{k}} \cdot \mathbf{J}_{n'} \cdot (\mathbf{J}_n^* - \hat{\mathbf{k}}\hat{\mathbf{k}} \cdot \mathbf{J}_n^*) = 0. \qquad (22)$$

By using (22) in (21) and by rearranging the dyadic products, one obtains:

$$\mathbf{J}_{n'} \cdot [\underline{\underline{\mathbf{I}}} - \hat{\mathbf{k}}\hat{\mathbf{k}}] \cdot \mathbf{J}_n^* . \qquad (23)$$

Appendix B
Analytical Expression of the Visible Green's Function

In this Appendix, we derive a convenient analytical expression of the visible Green's function, which was defined in (9) as

$$\underline{\underline{\mathbf{g}}}^{\text{vis}}(\mathbf{r}) = \frac{-k^2\zeta}{16\pi^2} \iint_{4\pi} [\underline{\underline{\mathbf{I}}} - \hat{\mathbf{k}}\hat{\mathbf{k}}] e^{-jk\hat{\mathbf{k}}\cdot\mathbf{r}} d\hat{\mathbf{k}} . \qquad (24)$$

Recalling the following property for the plane-wave spectral representation

$$\hat{\mathbf{k}}\hat{\mathbf{k}} e^{-jk\hat{\mathbf{k}}\cdot\mathbf{r}} = -\frac{\nabla\nabla}{k^2} e^{-jk\hat{\mathbf{k}}\cdot\mathbf{r}} \qquad (25)$$

and inverting the dyadic operator with the integrals, we can express the visible Green's function as

$$\underline{\underline{\mathbf{g}}}^{\text{vis}}(\mathbf{r}) = \frac{-k^2\zeta}{16\pi^2} \left[\underline{\underline{\mathbf{I}}} + \frac{\nabla\nabla}{k^2}\right] \iint_{4\pi} e^{-jk\hat{\mathbf{k}}\cdot\mathbf{r}} d\hat{\mathbf{k}} . \qquad (26)$$

This article has been accepted for publication in a future issue of this journal, but has not been fully edited. Content may change prior to final publication. Citation information: DOI 10.1109/TAP.2021.3090536, IEEE Transactions on Antennas and Propagation

The integral figuring in (26) can be closed according to what is demonstrated in Appendix C, thus $\underline{\underline{\mathbf{g}}}^{\text{vis}}$ can be written as follows

$$\underline{\underline{\mathbf{g}}}^{\text{vis}}(\mathbf{r}) = -\frac{\zeta}{4\pi}\left[k^2\underline{\underline{\mathbf{I}}} + \nabla\nabla\right]\text{sinc}(kr)\,. \tag{27}$$

APPENDIX C

In the present Appendix we would like to prove the following integral identity:

$$\int_0^{2\pi}\int_0^{\pi} e^{-jk\hat{\mathbf{k}}\cdot\mathbf{r}}\sin\theta d\theta d\phi = 4\pi\,\text{sinc}(kr). \tag{28}$$

Since $\mathbf{r}$ and $\hat{\mathbf{k}}$ can be written as

$$\mathbf{r} = r(\sin\theta\cos\phi\hat{\mathbf{x}} + \sin\theta\sin\phi\hat{\mathbf{y}} + \cos\theta\hat{\mathbf{z}}) \tag{29}$$

$$\hat{\mathbf{k}} = (\sin\beta\cos\alpha\hat{\mathbf{x}} + \sin\beta\sin\alpha\hat{\mathbf{y}} + \cos\beta\hat{\mathbf{z}}) \tag{30}$$

the left hand side of equation (28) can be rewritten as follows:

$$\int_0^{\pi} e^{jrk\cos\beta\cos\theta}\sin\theta\left[\int_0^{2\pi} e^{jrk\sin\beta\sin\theta\cos(\alpha-\phi)}d\phi\right]d\theta. \tag{31}$$

According to [29], the integral in brackets can be closed in:

$$2\pi\int_0^{\pi} e^{jrk\cos\beta\cos\theta}J_0(kr\sin\beta\sin\theta)\sin\theta d\theta \tag{32}$$

where J_0 is the zeroth order Bessel function of first kind. By using the asymptotic expansion of J_0 given in [29] and by using trigonometric identities, (32) becomes:

$$\pi e^{-j\frac{\pi}{4}}\int_0^{\pi}\sqrt{\frac{2}{\pi kr\sin\beta\sin\theta}}e^{jkr\cos(\beta-\theta)\sin\theta}d\theta + \pi e^{j\frac{\pi}{4}}\int_0^{\pi}\sqrt{\frac{2}{\pi kr\sin\beta\sin\theta}}e^{-jkr\cos(\beta+\theta)\sin\theta}d\theta. \tag{33}$$

By applying the stationary phase point method, (33) can be rewritten as:

$$\pi e^{-j\frac{\pi}{4}}\sqrt{\frac{2}{\pi kr\sin\beta\sin\theta'_s}}\sin\theta'_s\int_0^{\pi} e^{jkr\cos(\beta-\theta)}d\theta + \pi e^{j\frac{\pi}{4}}\sqrt{\frac{2}{\pi kr\sin\beta\sin\theta''_s}}\sin\theta''_s\int_0^{\pi} e^{-jkr\cos(\beta+\theta)}d\theta \tag{34}$$

where θ'_s and θ''_s are the saddle points of the phase functions figuring in the first and in the second integral respectively. By forcing the derivatives of these phase functions to be null, the stationary phase points can be found:

$$\theta'_s = \pm\beta, \qquad \theta''_s = \mp\beta \tag{35}$$

Since for both saddle points the solution must be an element in the integration domain $[0, 2\pi]$, it follows that:

$$\theta'_s = \theta''_s = \beta. \tag{36}$$

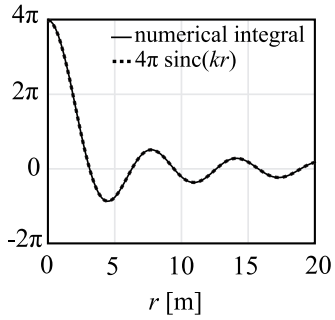

Fig. 15. Comparison between (28) evaluated numerically and its analytical solution (i.e. $4\pi\,\text{sinc}(kr)$), for $k = 1\,\text{m}^{-1}$.

By substituting (36) in (34), one obtains:

$$\pi e^{-j\frac{\pi}{4}}\sqrt{\frac{2}{\pi kr}}\int_0^{\pi} e^{jkr\cos(\beta-\theta)}d\theta + \pi e^{j\frac{\pi}{4}}\sqrt{\frac{2}{\pi kr}}\int_0^{\pi} e^{-jkr\cos(\beta+\theta)}d\theta \tag{37}$$

As reported in [29], both integrals can be closed into zeroth order Bessel functions of the first kind, by using their asymptotic expansion (37) becomes:

$$\pi e^{-j\frac{\pi}{4}}\sqrt{\frac{2}{\pi kr}}e^{-j\frac{\pi}{4}}\sqrt{\frac{2\pi}{kr}}e^{jkr} + \pi e^{j\frac{\pi}{4}}\sqrt{\frac{2}{\pi kr}}e^{j\frac{\pi}{4}}\sqrt{\frac{2\pi}{kr}}e^{-jkr}. \tag{38}$$

Calculating the products of (38) and then using Euler's identities leads to:

$$4\pi\frac{\sin(kr)}{kr} = 4\pi\,\text{sinc}(kr) \tag{39}$$

which proves the identity (28).

REFERENCES

[1] E. G. Larsson, O. Edfors, F. Tufvesson, and T. L. Marzetta, "Massive MIMO for next generation wireless systems," *IEEE Comm. Mag.*, vol. 52, no. 2, pp. 186-195, February 2014.

[2] W. Xiang, K. Zheng, and K. Shen, Eds., *5G mobile communications.* Springer Int.Publishing, Switzerland, 2017.

[3] W. Hong et al., "Multibeam antenna technologies for 5G wireless communications," *IEEE Trans. Antennas Propag.*, vol. 65, no. 12, pp. 6231-6249, Dec. 2017.

[4] J. Allen, "A theoretical limitation on the formation of lossless multiple beams in linear arrays," *IRE Trans. Antennas Propag.*, vol. 9, no. 4, pp. 350–352, Jul. 1961.

[5] W. White, "Pattern limitations in multiple-beam antennas," *IRE Trans. Antennas Propag.*, vol. 10, no. 4, pp. 430-436, Jul. 1962.

[6] S. Stein, "On cross coupling in multiple-beam antennas," *IRE Trans. Antennas Propag.*, vol. 10, no. 5, pp. 548–557, Sep. 1962.

[7] R.G. Vaughan, and J.B. Andersen, "Antenna diversity in mobile communications," *IEEE Trans. Vehicular Tech.*, vol. 36, no. 4, pp. 149-172, Nov. 1987.

[8] S. Blanch, J. Romeu, and I. Corbella, "Exact representation of antenna system diversity performance from input parameter description," *Electron. Lett.*, vol. 39, no. 9, pp. 705–707, May 2003.

[9] S. M. Mikki and Y. M. M. Antar, "On cross correlation in antenna arrays with applications to spatial diversity and MIMO systems," *IEEE Trans. Antennas Propag.*, vol. 63, no. 4, pp. 1798-1810, Apr. 2015.

[10] D. Sarkar, and S. M. Mikki, and Y. M. M. Antar, "An efficient analytical evaluation of the electromagnetic cross correlation Green's function in MIMO systems," *IEEE Trans. Antennas Propag.*, vol. 67, no. 11, pp. 6947-6956, Nov. 2019.

[11] P. N. Fletcher, M. Dean, and A. R. Nix, "Mutual coupling in multi-element array antennas and its influence on MIMO channel capacity," *Electron. Lett.*, vol. 39, no. 4, pp. 342-344, Feb. 2003.

[12] X. Li and Z.-P. Nie, "Mutual coupling effects on the performance of MIMO wireless channels," *IEEE Antennas Wirel. Propag. Lett.*, vol. 3, pp.344-347, 2004.

[13] B. Wang, Y. Chang, and Y. Sun, "Performance of the large-scale adaptive array antennas in the presence of mutual coupling," *IEEE Trans. Antennas Propag.*, vol. 64, no. 6, pp. 2236-2245, Jun. 2016.

[14] X. Chen, S. Zhang, and Q. Li, "A review of mutual coupling in MIMO systems," *IEEE Access*, vol. 6, pp. 24706-24719, Apr. 2018.

[15] Z. Li, Z. Du, M. Takahashi, K. Saito, and K. Ito, "Reducing mutual coupling of MIMO antennas with parasitic elements for mobile terminals," *IEEE Trans. Antennas Propag.*, vol. 60, no. 2, pp. 473-481, Feb. 2012.

[16] I. Nadeem and D. Choi, "Study on mutual coupling reduction technique for MIMO antennas," *IEEE Access*, vol. 7, pp. 563-586, 2019.

[17] H. Steyskal and J. S. Herd, "Mutual coupling compensation in small array antennas," *IEEE Trans. Antennas Propag.*, vol. 38, no. 12, pp. 1971-1975, Dec. 1990.

[18] S. Bellofiore, C. A. Balanis, J. Foutz, and A. S. Spanias, "Smart-antenna systems for mobile communication networks. Part I: Overview and antenna design," *IEEE Antennas Propag. Mag.*, vol. 44, no. 3, pp. 145-154, Jun. 2002.

[19] F. De Flaviis, L. Jofre, J. Romeu, and A. Grau, *Multiantenna Systems for MIMO Communications.* Williston, VT, USA: Morgan & Claypool, 2008.

[20] A. Ludwig, "Mutual coupling, gain and directivity of an array of two identical antennas," *IEEE Trans. Antennas Propag.*, vol. 24, no. 6, pp. 837-841, Nov. 1976.

[21] I. Tzanidis, G. Z. Hutcheson, Y. Li, J. Oh, W. Hong, G. Xu, and J. Zhang, "Method and apparatus for miniaturization of mimo systems via tightly coupled antenna array", U.S. patent no. US 2014/0334565 A1, Nov. 2014.

[22] T. K. Sarkar, "A note on the choice weighting functions in the method of moments," *IEEE Trans. Antennas Propag.*, vol. AP-33, no. 4, pp. 436-441, Apr. 1985.

[23] W. Wasylkiwskyj, and W. K. Kahn, "Theory of mutual coupling among minimum-scattering antennas," *IEEE Trans. Antennas Propag.*, vol. AP-18, no. 2, pp. 204-216, March 1970.

[24] W. K. Kahn, "Impedance-match and element-pattern constraints for finite arrays," *IEEE Trans. Antennas Propag.*, vol. 25, no. 6, pp. 747-755, Nov. 1977.

[25] R. F. Harrington, *Field Computation by Moment Methods*, Wiley - IEEE Press, 1993.

[26] C. Yepes, E. Gandini, S. Monni, A. Neto, F. E. van Vliet, and D. Cavallo, "Analysis of tilted dipole arrays: Impedance and radiation properties," *IEEE Trans. Antennas Propag.*, vol. 68, no. 1, pp. 254-265, Jan. 2020.

[27] D. Cavallo, W. H. Syed, and A. Neto, "Connected-slot array with artificial dielectrics: A 6 to 15 GHz dual-pol wide-scan prototype," *IEEE Trans. Antennas Propag.*, vol. 66, no. 6, pp. 3201-3206, Jun. 2018.

[28] D. Cavallo, W. H. Syed, and A. Neto, "Equivalent transmission line models for the analysis of edge effects in finite connected and tightly coupled arrays," *IEEE Trans. Antennas Propag.*, vol. 65, no. 4, pp. 1788-1796, Apr. 2017.

[29] M. Abramowitz and I. A. Stegun, *Handbook of Mathematical Functions with Formulas, Graphs, and Mathematical Tables.* New York: Dover Publications, Inc., 1964.

Riccardo Ozzola (S'20) received his B.Sc and M.Sc degree with honors from the University of Florence, Florence, Italy, in 2017 and 2019, respectively. His master thesis was carried out at the Terahertz Sensing Group of the Delft University of Technology (TU Delft), Delft, The Netherlands.

He is currently a PhD candidate at the Terahertz Sensing Group of TU Delft. His research interests include theory and design of multi-beam arrays and wideband arrays for wireless communication.

Daniele Cavallo (S'09−M'11−SM'19) received the M.Sc. degree (*summa cum laude*) in telecommunication engineering from the University of Sannio, Benevento, Italy, in 2007, and the Ph.D. degree (*cum laude*) in electromagnetics from Eindhoven University of Technology (TU/e), Eindhoven, The Netherlands, in 2011.

From 2007 to 2011, he was with the Antenna Group, Netherlands Organization for Applied Scientific Research (TNO), The Hague, The Netherlands. From 2012 to 2015, he was Post-Doctoral Researcher with the Microelectronics Department, Delft University of Technology (TU Delft), Delft, The Netherlands. In 2015, he joined Chalmers University of Technology, Gothenburg, Sweden, as a Visiting Researcher. He is currently an Associate Professor with the Terahertz Sensing Group, TU Delft. He has authored or coauthored around 150 papers published in peer-reviewed international journals and conference proceedings. His current research interests include analytical and numerical methods for antenna characterization, the design of antenna arrays, and on-chip antennas.

Dr. Cavallo was a recipient of the Best Innovative Paper Prize at the 30th ESA Antenna Workshop in 2008, the Best Paper Award in Electromagnetics and Antenna Theory at the 11th European Conference on Antennas and Propagation (EuCAP) in 2017, and the Three-Year Personal Grant from the Netherlands Organization for Scientific Research (NWO VENI, 250 keuro), for developing "Efficient On-Chip Antennas for Terahertz Applications." His students received the Best Student Paper Award at EuCAP 2013, the Special Mention at EuCAP 2015, and the Else Kooi Prize in 2016. He is currently an Associate Editor of the IEEE TRANSACTIONS ON ANTENNAS AND PROPAGATION. He is a member of the European Association on Antennas and Propagation (EurAAP) and co-coordinator of the EurAAP working group "Active Array Antennas" .

Andrea Neto (Fellow, IEEE) received the Laurea degree (summa cum laude) in electronic engineering from the University of Florence, Florence, Italy, in 1994, and the Ph.D. degree in electromagnetics from the University of Siena, Siena, Italy, in 2000. Part of his Ph.D. degree was developed at the European Space Agency Research and Technology Center Noordwijk, The Netherlands. He worked for the Antenna Section at the European Space Agency Research and Technology Center for over two years. From 2000 to 2001, he was a Post-Doctoral Researcher with the California Institute of Technology, Pasadena, CA, USA, where he worked with the Submillimeter Wave Advanced Technology Group. From 2002 to January 2010, he was a Senior Antenna Scientist with TNO Defense, Security, and Safety, The Hague, The Netherlands. In February 2010, he became a Full Professor of applied electromagnetism with the EEMCS Department, Technical University of Delft, Delft, The Netherlands, where he formed and leads the THz Sensing Group. His research interests include the analysis and design of antennas with an emphasis on arrays, dielectric lens antennas, wideband antennas, EBG structures, and THz antennas. Dr. Neto served as an Associate Editor for the IEEE TRANSACTIONS ON ANTENNAS AND PROPAGATION (2008–2013) and IEEE ANTENNAS AND WIRELESS PROPAGATION LETTERS (2005–2013). He is a member of the Technical Board of the European School of Antennas and organizer of the course on antenna imaging techniques. He is a member of the Steering Committee of the Network of Excellence NEWFOCUS, dedicated to focusing techniques in mm and submillimeter wave regimes. In 2011, he was a recipient of the European Research Council Starting Grant to perform research on Advanced Antenna Architectures for THz Sensing Systems. He was a recipient of the H. A. Wheeler Award for the best applications paper of 2008 in the IEEE TRANSACTIONS ON ANTENNAS AND PROPAGATION, the Best Innovative Paper Prize of the 30th ESA Antenna Workshop in 2008, and the Best Antenna Theory Paper Prize of the European Conference on Antennas and Propagation (EuCAP) in 2010. In 2011, he was a recipient of the European Research Council Starting Grant to perform research on advanced antenna architectures for THz sensing systems.